Archive of Applied Mechanics manuscript No.
(will be inserted by the editor)

Su Zhao · Jörg Wallaschek

A standing wave acoustic levitation system for large planar objects

Received: date / Accepted: date

Abstract An acoustic levitation system is presented in this paper which can levitate planar objects much larger than the wavelength of the applied sound wave. It uses standing wave field formed by the sound radiator and the levitated planar object. An experimental setup is developed, by which a compact disc is successfully levitated at frequency of 19 kHz and input power of 40 W. The sound field is modeled according to acoustic theory. The mean excess pressure experienced by the levitated object is calculated and compared with experiment results. The influences of the nonlinear effects within the acoustic near-field are discussed. Nonlinear absorption coefficient is introduced into the linear model to give a more precise description of the system. The levitation force is calculated for different levitation distances and driving frequencies. The calculation results show acceptable agreement with the measurement results.

Keywords Acoustic levitation · standing wave · acoustic radiation pressure

1 Introduction

Levitation is a process by which an object is suspended in a stable position against gravity, without physical contact. Levitation can be realized by various physical means, such as magnetic force, electrostatic force, aerodynamic force, acoustic radiation force and so on. In this paper, one dimensional levitation methods utilizing high intensive ultrasonic sound waves are discussed. An acoustic wave can exert a force on objects immersed in the wave field. These forces are normally weak, but they can become quite large when using high intensity waves due to the nonlinear characteristics. The forces can even be large enough to levitate substances against gravity force. This technique is called acoustic levitation or ultrasonic levitation, when the sound waves used are in the ultrasonic frequency range (higher than 20 kHz).

1.1 Different configurations of acoustic levitation

According to the working principles, two different configurations of acoustic levitation can be found in the literature: standing wave levitation and squeeze film levitation (also called as near field acoustic

S. Zhao
Institute for Dynamics and Vibration Research, Appelstr. 11, 30167 Hannover, Germany
Tel.: +49-511-7623166
Fax: +49-511-7624164
E-mail: zhao@ids.uni-hannover.de

J. Wallaschek
Institute for Dynamics and Vibration Research, Appelstr. 11, 30167 Hannover, Germany

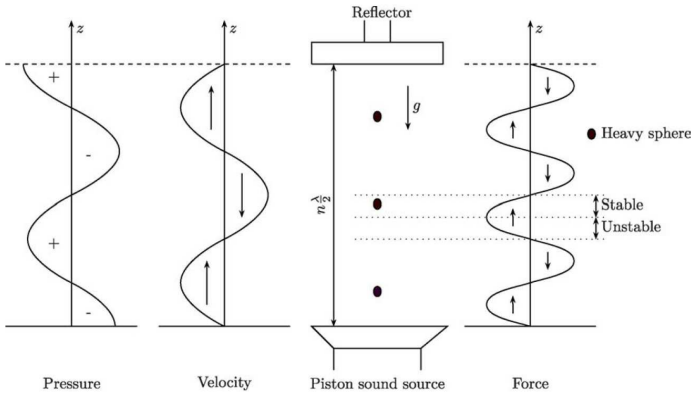

Fig. 1 Distribution of sound pressure, air particles's velocity and levitation force in a standing wave type levitation system[38]

levitation) [38]. Standing wave levitation phenomenon was first observed in Kundt's tube experiment [29] in 1866, that small dust particles moved toward the pressure nodes of the standing wave created in a horizontal Kundt's tube. Bücks and Müller presented an experiment setup for acoustic levitation in 1933 [6]. A small particle was levitated at a position slightly below the pressure nodes of the standing wave between a radiator and a reflector.

A typical setup for standing wave levitation is shown in Fig. 1. As a result of multiple reflections between an ultrasonic radiator and a solid, flat or concave reflector, a standing wave with equally spaced nodes and anti-nodes of the sound pressure and velocity amplitude will be generated. Solid or liquid samples with effective diameters less than a wavelength can be levitated below the pressure nodes. The axial suspension of the sample is an effect of the sound radiation pressure of a standing wave. Combining with a Bernoulli vacuum component, the sound wave can locate the samples laterally as well [9].

Following this radiator-reflector idea, standing wave type acoustic levitators with various features were designed for applications in different scientific disciplines such as space engineering, non-contact material processing and non-contact handling. In 1974, Wang et. al. [39] presented an acoustic chamber for positioning of molten materials. The chamber was used for positioning in an extreme temperature gradient. In 1975, Whymark [43] proposed an acoustic levitator for positioning of materials in space using a single source of sound. In 1983 Lierke [21] presented an acoustic levitator for positioning the materials samples in mirror furnaces in space processing. In 1985, Trinh [36] presented a compact acoustic levitation device for studies in fluid dynamics and materials science in the laboratory and in microgravity. The classic structure was later modified to achieve better performances. Otsuka et. al. [28] used a stepped circular vibrating plate as the radiator which can produce higher intensity ultrasound fields. The flexural vibration mode of the plate with two nodal circles was used to achieve higher vibration amplitude. In 2001, Xie and Wei [45] enhanced the standing wave acoustic levitation force by properly curving the surface and enlarging the reflector. High density material like tungsten ($\rho = 18.92$ g/cm^3) was successfully levitated for the first time by standing wave ultrasonic levitation. Recently in 2006, Xie and Wei reported the successful levitation of small living animals such as ant, ladybug, and little fish with a standing wave acoustic levitator [47].

Squeeze film levitation is observed when an object with a flat surface is placed directly upon a sound radiator. The object can be levitated very close to the radiation surface, at a height which is much smaller than the wavelength of the applied sound wave. In 1964, Salbu [33] described a levitation system for objects with flat surface. Salbu used magnetic actuators to excite two conforming surfaces oscillating next to each other to generate a positive load supporting force. Linear and journal bearings based on this levitation method were presented in Salbu's publication. In 1975, Whymark [43] reported that a brass planar disk of 50 mm in diameter and 0.5 mm in thickness was levitated extremely close to a piston vibration source driven harmonically at a frequency of 20 kHz. Two distinct properties distinguish this type of levitation from standing wave levitation. First, the reflector is no longer needed;

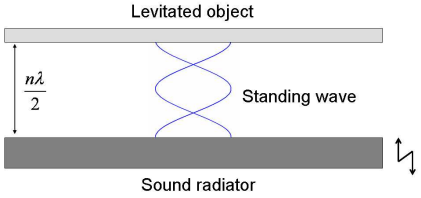

Fig. 2 Schematic diagram of the proposed acoustic levitation system

instead, the levitated object itself acts as an obstacle for the free propagation of the ultrasonic wavefront. Second, the gap between radiation source and the levitated object must be much smaller than the sound wavelength in air. Thus, standing wave does not exist in the gap anymore. Several levitation systems have been developed using squeeze film levitation technique [11; 17; 25; 44; 37; 16; 14]. This kind of systems has also been investigated for non-contact transportation of electronic parts (e. g. wafer handling) using traveling bending waves [15; 31].

1.2 A configuration of acoustic levitation for large planar objects

In 2001, Reinhart [31] reported that while measuring the squeeze film levitation force, additional peaks of levitation force at intervals of half wavelengths from the radiation surface were also observed. These additional peaks had much smaller amplitudes ($< 0.1N$) compared to the squeeze-film region. Reinhart concluded that they were caused by the standing wave pattern and pointed out a possibility of levitating planar objects at these points. But no further explanation or experimental investigation was reported afterwards.

In this paper, an acoustic levitation system is investigated using the levitation effect observed by Reinhart. The levitation happens when planar objects are placed at distances of half wavelengths in front of a radiator. A schematic diagram of the proposed levitation system is shown in Fig. 2. In this configuration, the levitation effect is achievable using similar setup of standing wave or squeeze levitation, but the working principle is different in many aspects. First, the acoustic field is formed in between the sound radiator and the levitated object which performs as a reflector as in classic standing wave levitation systems. The position of the object to be levitated determines how the sound field is maintained. Second, the size of the object to be levitated is not limited by the wavelength, because the object is levitated above the complete standing wave field. In the classic standing wave levitation, the small particles are trapped stably slightly under a pressure node or anti-node of a standing wave field formed by a radiator and a reflector. Thus, the particles can only be levitated if they are smaller than a sound wavelength. At last, as compared to squeeze film levitation, the object can be levitated at positions of multiple times of half wavelength above the radiator. A stable levitation happens when a standing wave is formed between the radiator and the object. However, the squeeze film levitation happens only when the object is place extremely close to the radiator. Thus no standing wave is formed in the gap.

The most renowned models of standing wave and squeeze film type acoustic levitations are reviewed in Sec. 2. Mathematical modeling based on the acoustic radiation theory is presented in Sec. 3. The levitation force for the proposed system is calculated. A experimental setup is developed and presented in Sec. 4 to validate the proposed levitation method. Sound field visualization of the proposed system is presented in Sec. 4.1. Simulation results based on the mathematical model are presented in Sec. 5.

2 Previous works on modeling the acoustic levitation systems

Various models have been developed to study the acoustic levitation systems. An major purpose of the models is to predict the levitation force. Acoustic radiation pressure is found to be the major source of

the levitation forces. Acoustic radiation pressure is a topic of nonlinear acoustics which was first studied by Rayleigh [30] in 1902 as an acoustic counterpart of electromagnetic waves. The radiation pressure on the object in the sound field varies with the frequency of the vibrations and equals zero in a linear approximation. A second order approximation is needed to obtain a non-zero mean pressure, which is small compared to the sound pressure amplitude [1]. The radiation pressure is a nonlinear effect comes from the nonlinearity of the adiabatic equation of state [19] (with allowance of the quadratic terms)

$$p = P - P_0 = A\left(\frac{\rho-\rho_0}{\rho_0}\right) + \frac{B}{2}\left(\frac{\rho-\rho_0}{\rho_0}\right)^2 \tag{1}$$

and the convection term of the Euler equation[1] for a non-viscous Newtonian fluid

$$\rho\frac{\partial \mathbf{v}}{\partial t} + \rho\left(\mathbf{v}\cdot\boldsymbol{\nabla}\right)\mathbf{v} = -\boldsymbol{\nabla}p \tag{2}$$

where P_0 is the ambient pressure; $P = P_0 + p$, in which p is the acoustic pressure; ρ_0 is the ambient density; $\rho = \rho_0 + \rho'$, in which ρ' is the acoustic density; Γ is a constant; and $\mathbf{v}$ is the velocity. For an ideal gas, $\Gamma = \gamma$, in which γ represents a specific heat ratio. A, B are called nonlinearity parameters, $A = \rho_0 c_0^2$, $B = (\Gamma-1)\rho_0 c_0^2$ and $B/A = \Gamma - 1$. From these basic equations, the subject has been investigated by many researchers with different results and had been continued to be associated with a lot of confusion for a few decades, mainly because the phenomenon involves a subtle nonlinear effect that the problem has to be very carefully posed in order to get a unique answer [7].

In 1982, Chu and Apfel [8] calculated the forces produced by a sound beam directed normally at a plane target. The author also pointed out several mistakes in previous theories and calculated the Rayleigh radiation pressure in an ideal gas on a perfectly reflecting target as:

$$p_{ra} = \frac{1+\gamma}{2}\left(1 + \frac{\sin(2kh)}{2kh}\right)\langle E\rangle \tag{3}$$

Here, E is the energy density of the wave. The angle brackets indicate that the parameters in them are time averaged. The time averaged energy density can be expressed as

$$\langle E\rangle = \left(a_0^2/4\right)\left(\rho_0\omega^2/\sin^2 kh\right) \tag{4}$$

where ω represents the angular frequency of the wave, a_0 the vibration amplitude and h the distance between vibration source and target. k represents the wave number $k = \omega/c$, in which c is the sound speed. Chu and Apfel also calculated the Rayleigh radiation pressure on partially reflecting plane targets. However, their calculation was limited to plane waves.

In 1993, Lee and Wang [19] used Eulerian coordinates instead of the previously used Lagrangian coordinates and extended the theory to general 3-D systems. The author stated that, for 1-D case, if the the material surface vibrates with sound, the mean pressure on it is Lagrangian. In the case of a rigid surface, the mean pressure on it becomes Eulerian. The mean Eulerian excess pressure was obtained as:

$$\left\langle P^E - P_0\right\rangle = \langle V\rangle - \langle K\rangle + C \tag{5}$$

in which V and K are the potential and kinetic energy densities of the considered wave, which are given as

$$V = \frac{1}{2}\frac{1}{\rho_0 c^2}p^2 \tag{6}$$

$$K = \frac{1}{2}\rho_0 v^2 \tag{7}$$

C is a constant and can be given a finite value to satisfy different boundary conditions on the system, or set to zero if there is none.

The mean pressure on the surface of the reflector is then the acoustic radiation pressure we are looking for. The acoustic radiation pressure has to be integrated over the object surface to obtain the

levitation force. However, in different types of levitation systems, different boundary conditions and calculation methods are needed. And, the considered levitated objects are very unlike.

For standing wave levitators, the part to be handled is usually small (effective radius smaller than the wavelength, mm-range) and immersed in a standing wave field. Radiation pressures acting on all surfaces on the levitated object must be figured out and summed. The first detailed theoretical description of standing wave levitation was given by King [18]. King assumed the fluid being adiabatic and barotropic. The acoustic radiation force on a rigid sphere was calculated by King as:

$$F = -\frac{5}{6}\pi\rho_0 |A|^2 (kR_s)^3 \sin(2kh) \tag{8}$$

in which ρ represents the density of the medium, R_s the radius of the sphere and $|A|$ the amplitude of the velocity potential.

King's work was extended by Hasegawa and Yosioka [13] to include the effects of compressibility. Embleton [10] adopted King's approach to fit to the case of a rigid sphere in a progressive spherical or cylindrical wave field. Westervelt [40; 41; 42] derived a general expression for the force owing to radiation pressure acting on an object of arbitrary shape and normal boundary impedance. King showed that a boundary layer with a high internal loss can lead to forces that are several orders of magnitude greater than those predicted by the classical radiation pressure theory.

A very different approach compared to King was presented by Gor'kov [12], who presented a simple method to determine the forces acting on a particle in an arbitrary acoustic field. The velocity potential was represented as sum of an incident ϕ_{in} and a scattered term ϕ_{sc}. Barmatz [2] applied Gor'kov's method to derive the generalized potential and force expressions for arbitrary standing wave modes in rectangular cylindrical and spherical geometries. Lierke gave an overview of standing wave acoustic levitation in 1996 [20] based on long term research and development activities for the European and the US space agencies. In 2004, Xie and Wei [46] studied the acoustic levitation force on disk samples and the dynamics of large water drops in a planar standing wave, by solving the acoustic scattering problem through incorporating the boundary element method.

For squeeze film levitation, the levitated object must have a planar surface, and is placed extremely close (μm-range) to the radiation source. Moreover, the standing wave does not exist any more. Instead, a very thin air film with pressure varying according to the movement of the radiation surface is to be considered. Due to the different boundary conditions, the analytical calculation of the levitation force is very different from the case of the standing wave levitation. Mathematical models for calculating the levitation force of squeeze film levitation can be derived from acoustic radiation pressure theory as well by considering the special physical conditions [14; 27]. Recalling Equ. (3), in squeeze film levitation, the levitation distance h is much smaller than the wavelength of sound λ, ranges from several to several tens microns. Therefore, $kh = 2\pi/\lambda << 1$ and $\sin kh \approx kh$ are approximately valid. Equ. (3) can be simplified to a linear equation for the radiation pressure in squeeze film levitation [14]:

$$\Pi = \frac{1+\gamma}{4}\rho_0 c^2 \frac{a_0^2}{h^2} \tag{9}$$

From Equ. 9, it is clear to see that the radiation pressure Π in squeeze film levitation is reversely proportional to the square of the levitation distance and proportional to the square of the vibration amplitude a_0. The radiation pressure reaches its maximum when the average levitation distance h equals the vibration amplitude a_0, right before a contact could happen. There are also models developed using the theory of gas film lubrication by solving variants of the Reynolds equation numerically or analytically. Such models give the exact pressure distributions along the gap. Detailed the explanations can be found in Ref. [33; 26; 35; 48].

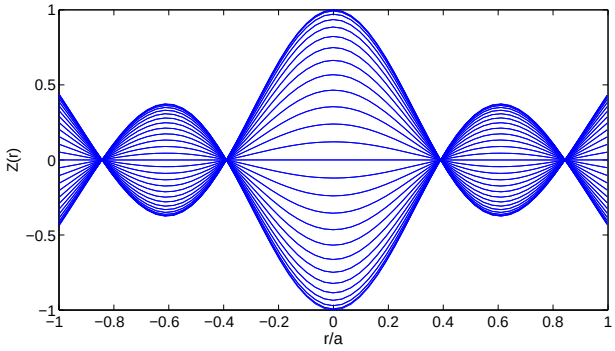

Fig. 3 Vibration amplitude distribution on the radiator surface

3 Modeling of the proposed levitation system

The intention of the proposed acoustic levitation system is to levitate a disc-shaped object with relative large size (a few times of the sound wavelength in air). In order to obtain a large sound radiation surface, a circular plate which vibrates in its flexural vibration mode is chosen as the sound radiator. The sound field to be considered can be simplified and described as following: the sound radiator (a circular disc) vibrates in its flexural vibration mode and generates a sound beam in front of it. The sound beam propagates forwards and is reflected by a rigid surface (the object to be levitated) placed perpendicular to the sound beam at a distance of L away from the radiator. A acoustic wave field resulted from multiple reflections is formed between two surfaces. The acoustic field becomes a standing wave when L is equal to multiple times of half wavelength of sound (as shown in Fig. 2). Excessive pressure on the rigid surface is generated by the acoustic field.

3.1 Flexural vibration mode of the radiator

The selected sound radiator is a circular plate with constant thickness. Therefore, cylindrical coordinates (r, θ, z) can be used, where r is a radius from the center, θ the angle of that radius, and z a length in the direction normal to the plane of the radiator. The plate equation has the following general solution for the transverse vibration mode of a circular plate[5]

$$Z(r,\theta,t) = \left[a_{ij}\mathrm{J}_i\left(\frac{\lambda_{ij}r}{a}\right) + b_{ij}\mathrm{I}_i\left(\frac{\lambda_{ij}r}{a}\right)\right]\cos i\theta\ \cos 2\pi ft \tag{10}$$

where $Z(r,\theta)$ is the displacement of the mid-surface of the plate, a the radius of the circular plate, f the natural frequency of the related mode shape. i and j are the number of nodal diameters and nodal circles(not counting the boundary) respectively. J_i and I_i are Bessel function and modified Bessel function of the first kind relatively, and i order. a_{ij} and b_{ij} are constants which are determined to within an arbitrary constant by the boundary conditions and mode number. λ_{ij} is a dimensionless frequency parameter related to the boundary conditions on the plate, the plate geometry and Poisson's ratio. For mode shapes with only nodal circles ($i = 0$) the displacement of the circular plate becomes axisymmetric. The displacement Z is then independent of θ. Equ. 10 can be simplified as

$$Z(r) = \left[a_{0j}\mathrm{J}_0\left(\frac{\lambda_{0j}r}{a}\right) + b_{0j}\mathrm{I}_0\left(\frac{\lambda_{0j}r}{a}\right)\right]\ \cos 2\pi ft \tag{11}$$

The vibration mode of a free circular plate with two nodal circles is shown in Fig. 3. Values of λ_{ij} of common mode shapes have been calculated and listed in Table $11-1$ in Ref. [5]. From this table, λ_{02} is found as 6.209. By applying the boundary conditions, a_{02} and b_{02} are determined as 0.997 and 0.003 respectively.

3.2 Sound beam in the acoustic near-field

According to Ref. [34], the acoustic far-field is approximately reached when z exceeds a^2/λ, where a is the radius of the radiator, and λ the wavelength of sound. For the proposed levitation system, the working frequency is about 20 kHz with wavelength λ being about 0.017 m. The radius of the sound radiator is 0.06 m. These makes $a^2/\lambda = 0.208$ m, which is about twelve times of λ. The investigated range of the levitation distance L is around one to a few times of half wavelengths. Therefore the considered sound field is completely located in the acoustic near-field.

A sound beam can be described in cylindrical coordinates with Bessel functions in r and sinusoidal function in z direction,

$$p(r, z, t) = A_0 \mathrm{J(r)}\ \cos(\omega t - kz) \tag{12}$$

where A_0 is the amplitude of acoustic pressure at $r = 0$, k the wave number, ω the angular frequency of the wave and z the distance from the vibration source. J(r) is the Bessel functions describing the radial distribution of the sound beam. For calculation it is convenient to use a complex number representation. Equ. 12 can be then written as

$$\mathbf{p}(r, z, t) = \mathrm{Re}\left(A_0 \mathrm{J(r)} e^{\mathbf{j}(\omega t - kz)}\right) \tag{13}$$

where Re indicates the real part of the expression. In the following Re will not be mentioned for simplification. All the complex parameters are automatically considered as their real parts.

Unlike a plane wave, in a sound beam described by Equ. 13, air particles move in both r and z directions. However, in the near-field, the acoustic field is basically cylindrical, the oscillations in the r direction are small compared to z direction and have very little contribution on the radiation pressure. Therefore, velocity component in r direction is not taken into account in the present model. A sound beam with the same diameter as the radiator is considered. Assuming that the acoustic pressure at the surface of the radiator varies exactly according to the transverse movement of the radiator, the Bessel functions in Equ. 12 can be replace by $Z(r)$. The sound beam in near-field can be then expressed as:

$$\mathbf{p}(r, z, t) = A_0 Z(r)\ e^{\mathbf{j}(\omega t - kz)} \tag{14}$$

The axial pressure at the center of a sound beam generated by a circular piston varies in the near-field and may have one or more maximums occur along the axis when $ka > \pi$. The pressure variations are extreme for a circular piston because of the high degree of symmetry [34]. For the circular plate with flexural mode as shown in Fig. 3, the fluctuation of axial pressure amplitude at the center is reduced by the nearly symmetric high and low pressure field on the plate. Therefore, the variation of the pressure amplitude A_0 is not as significant as the circular piston anymore, and is considered as constant in the near-field for the present model. The particle velocity in z direction is expressed as

$$\mathbf{v}(r, z, t) = \frac{A_0}{\rho_0 c}\ Z(r) e^{\mathbf{j}(\omega t - kz)} \tag{15}$$

3.3 Increased absorption due to nonlinear effects

When a sound wave travels through air, a proportion of the sound energy is converted to heat. There are heat conduction, shear viscosity and molecular relaxation losses. So the sound wave is absorbed by the air. The air absorption becomes significant at high frequencies and at long range [32]. For a plane wave, the pressure p at distance z from a position where the pressure is p_0 is given as

$$p = p_0 e^{-\alpha z} \tag{16}$$

The attenuation coefficient α for air absorption depends on frequency, humidity, temperature and atmospheric pressure and may be calculated as following[4; 3]:

$$\alpha = f^2 \left\{ 1.84 \times 10^{-11} \left(\frac{T}{T0}\right) \left(\frac{p_{s0}}{p_s}\right) + \left(\frac{T}{T_0}\right)^{-5/2} \left[0.01278 \frac{\exp(-2239.1/T)}{F_{rO} + f^2/F_{rO}} + 0.1068 \frac{\exp(-3352/T)}{F_{rN} + f^2/F_{rN}} \right] \right\} \tag{17}$$

where f represents the frequency of the wave, p_s the atmospheric pressure, p_{s0} the reference atmospheric pressure (1 atm), T the atmospheric temperature in K, T_0 the reference atmospheric temperature (293.15 K). f_{rO} and f_{rN} are the relaxation frequencies of the molecular oxygen and nitrogen, which can be calculated as,

$$f_{rO} = \frac{p_s}{p_{s0}} \left(24 + 4.04 \times 10^4 h \, \frac{0.02 + h}{0.391 + h} \right) \tag{18}$$

$$f_{rN} = \frac{p_s}{p_{s0}} \left(\frac{T_0}{T}\right)^{1/2} \left(9 + 280h \times \exp\left\{ -4.17 \left[\left(\frac{T_0}{T}\right)^{1/3} - 1 \right] \right\} \right) \tag{19}$$

respectively, where h is the absolute humidity in %. The relation between h and relative humidity h_r is

$$h = h_r \left(p_{sat}/p_{s0}\right) / \left(p_s/p_{s0}\right) \tag{20}$$

where the saturated vapor pressure p_{sat} is given by

$$log_{10} \frac{p_{sat}}{p_{s0}} = -6.8346 (T_{01}/T)^{1.261} + 4.6151 \tag{21}$$

where $T_{01} = 273.16\ K$ is the triple-point isotherm temperature.

The absorption coefficient α discussed here is calculated with linear assumptions. It fits to sound waves with pressure amplitude much smaller than the ambient air pressure ($A_0 << P_0$). However, in acoustic levitation systems, high intensity and high acoustic pressure amplitude are normally involved. Propagation of such finite-amplitude waves is accompanied with a variety of nonlinear effects whose intensity depends on the amplitude of vibrations, such as waveform distortion, formation of shock waves, increased absorption, nonlinear interaction, cavitation and sonoluminescence [32]. The waveform distortion always exits in nonlinear waves. They come from the generation of higher harmonics during propagation. The absorption increases dramatically for higher frequencies, therefore the distorted wave are absorbed more than the harmonic waves. A relation between the absorption of finite and small amplitude waves is given in Ref. [24] as:

$$\frac{\alpha'}{\alpha} = 1 + \frac{3\omega^2 v_0}{4\alpha c^2} \left(1 + \frac{B}{2A}\right) e^{-2\alpha z} \left(1 - e^{-2\alpha z}\right) \tag{22}$$

In which, α' represents the increased absorption coefficient of finite amplitude wave, v_0 the air particle speed amplitude, z the traveling distance. α' is now a function of the particle speed amplitude v_0 and increases as v_0 gets higher. When standing wave is formed, as a result of signified resonance, the air particle speed increases significantly. As a result, α' obtained from Equ. 22 can be significantly larger than α.

By substituting the attenuation coefficient into Equ.14 we obtain,

$$\mathbf{p}(r, z, t) = A_0 Z(r)\, e^{-\alpha' z + \mathbf{j}(\omega t - kz)} \tag{23}$$

3.4 Modeling the sound field

Consider the problem in which the plane wave described by Equ. 23 traveling in the z direction is reflected at $z = 0$ by a rigid fixed plane wall. The reflected wave is again reflected at the radiation surface located at $z = L$ and propagates toward the reflector. The reflection of the wave goes on and on between two rigid surfaces until the wave is totally absorbed by the air. The resulted sound field between the sound radiator and the reflector is the summation of all the foregoing and reflected waves. The infinite summation of such waves is proved to be equal to the summation of one foregoing and one reflected wave with same amplitude [15]. The resulted sound field can be described as

$$\mathbf{p}(r, z, t) = A_0 Z(r) \cdot (\cos kz \cdot \cosh \alpha' z + \mathbf{j} \sin kz \cdot \sinh \alpha' z)\, e^{\mathbf{j}\omega t} \tag{24}$$

The corresponding acoustic velocity $\mathbf{v}$ in z direction is expressed as

$$\mathbf{v}(r, z, t) = -\frac{A_0}{\rho_0 c} Z(r) \cdot (\cos kz \cdot \sinh \alpha' z + \mathbf{j} \sin kz \cdot \cosh \alpha' z)\, e^{\mathbf{j}\omega t} \tag{25}$$

Notice that only the near-field region is considered in this context, and the speed of air particles in r direction is ignored. So far, the representation of the entire cylindrical sound field is obtained. The next step is to calculated the radiation pressure produced by the obtained sound field.

Since the reflector surface is considered as rigid, the radiation pressure on is Eulerian [19]. Equ. 5 can be then applied to calculate the radiation pressure at the reflecting surface generated by the sound field described by Equ. 24. Substituting Equ. 24 and Equ. 25 in to Equ. 6 and Equ. 7, after time-averaging, $\langle V \rangle$ and $\langle K \rangle$ are obtained as

$$\langle V \rangle = \frac{A_0^2 Z(r)^2}{4\rho_0 c^2} \left(\cos^2 kz \ \cosh^2 \alpha' z - \sin^2 kz \ \sinh^2 \alpha' z\right) \tag{26}$$

$$\langle K \rangle = \frac{A_0^2 Z(r)^2}{4\rho_0 c^2} \left(\sin^2 kz \ \cosh^2 \alpha' z - \cos^2 kz \ \sinh^2 \alpha' z\right) \tag{27}$$

For a sound beam in free space there is no constrain to satisfy. Therefore, $C = 0$. Substituting Equ. 26 and Equ. 27 into Equ. 5, the mean Eulerian excess pressure is obtained as

$$P^E - P_0 = \langle V \rangle - \langle K \rangle = Z(r)^2 \frac{A_0^2}{4\rho_0 c^2} \cos 2kz \left(\sinh^2 \alpha' z + \cosh^2 \alpha' z\right) \tag{28}$$

Equ. 28 describes the mean excess pressure at fix points within the sound field. For a certain sound field, the mean excess pressure varies at different (r, z) positions. On the plane at $z = 0$ perpendicular to z, the mean pressure becomes the acoustic radiation pressure $p_r a$ on the object. $p_r a$ can be obtained by setting $z = 0$ in Equ. 28 as

$$p_r a = Z(r)^2 \frac{A_0^2}{4\rho_0 c^2} \tag{29}$$

p_{ra} is not uniform in r and distributes following function $Z(r)^2$.

4 Experimental investigations

A schematic diagram of the disc levitation system is shown in Fig. 4. A piezoelectric Langevin type transducer driven in its first longitudinal mode ($\lambda/2$) at 20 kHz is used to generate ultrasonic vibrations. A stepped horn ($\lambda/2$) is attached to magnify the vibration amplitude of the transducer. An aluminum plate of diameter 120 mm is used as sound radiator. The plate is screwed into the horn.

For matching one of the plate's axisymmetric flexural modes of vibration to the axial resonant frequency of horn and transducer, the plate-thickness is chosen so that the corresponding natural frequency of the free-vibrating plate appears at 20 kHz [22]. Flexural modes of vibration with one, two, and three nodal circles have been constructed by properly matching the thickness. Experimentally,

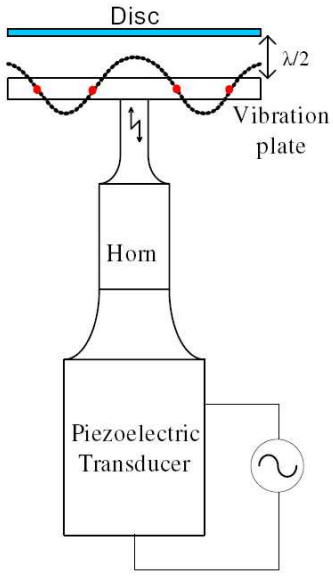

Fig. 4 Schematic diagram of the experiment setup of the proposed levitation system

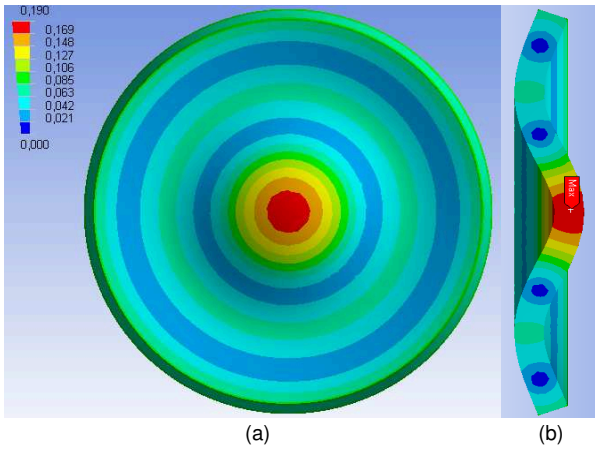

Fig. 5 Calculation of the flexural vibration mode of the circular plate with two nodal circles (FEM result). (a),front view, (b)cross-section view

a plate with two nodal circles is found to be a good compromise between mechanical strength and achievable vibration amplitude. The thickness of the plate is 8.55 mm. A result of a Finite-Element calculation of the vibration mode at 20 kHz with two nodal circles is shown in Fig. 5. The mode shape agrees with the calculation result (shown in Fig. 3) very well. After assembly, the resonant frequency of the entire system (transducer, horn, and plate) appears at about 19 kHz, slightly depending on the input power. An Adaptive Phase Locked Loop control algorithm (APLL) is used for tracking the resonant frequency of the system during operation [23].

An experimental setup is built up as shown in Fig. 6 to measure the levitation force produced by the presented disc levitation system. An aluminum plate with the same diameter as the radiation plate is positioned in opposite to the radiator. This sound-reflecting plate is mounted on a vertical linear stage through a load cell for being able to measure the vertical force acting on the reflector directly. Using the linear stage, the reflector may be positioned freely between the contact position and a distance of about 40 mm above the radiator. A laser interferometer is installed to measure the exact vertical position of the reflector.

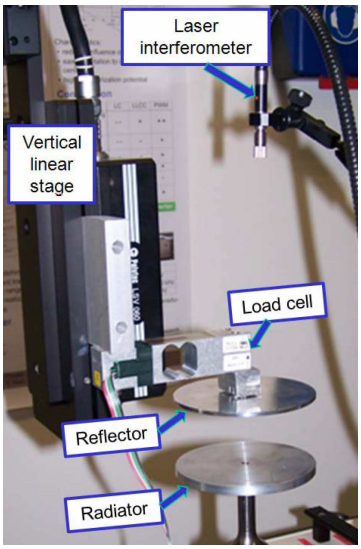

Fig. 6 Experiment setup for measuring the acoustic radiation force

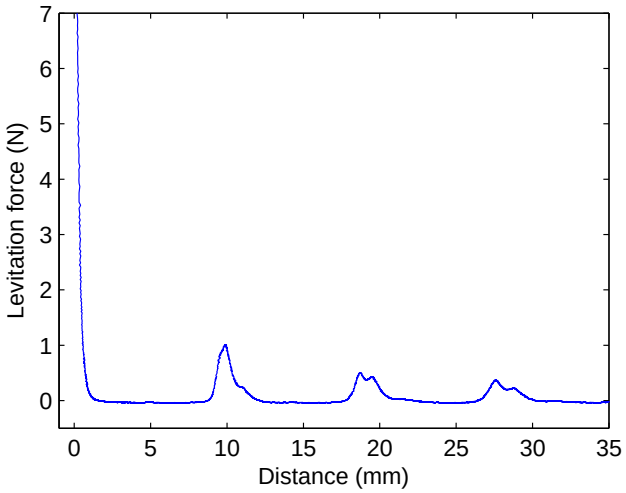

Fig. 7 Levitation force versus levitation distance. Input power 50 W, frequency 19 KHz.

Measurements have been done with fixed voltage input of 50 V at a frequency of 19 kHz (input power about 40 W). The actual vertical position data of the reflector and the value of the levitation force are recorded simultaneously while the reflector slowly approaches the radiator from above until both plates get into contact. Levitation force versus distance between the plates is plotted in Fig. 7. Clear peaks of the levitation force can be seen in Fig. 7 at intervals of half wavelengths. The peak-values at the positions of half wavelengths increase with decreasing distance between the plates. The amplitude at the $\lambda/2$-position is about 1 N. Multiple peaks are observed near the positions of half wavelengths. This is because the nonlinear behavior of such a intensive sound beam. The uneven pressure distribution along radial direction causes unequal sound speed. Therefore the standing wave is formed at slight different positions for different part the sound beam.

When the gap between the plates gets smaller than 0.5 mm, the squeeze-film region is reached and the levitation force starts to increase significantly. A maximum levitation force up to 100 N is measured right before contact happens. The squeeze film levitation force could be further increased by using polished surfaces.

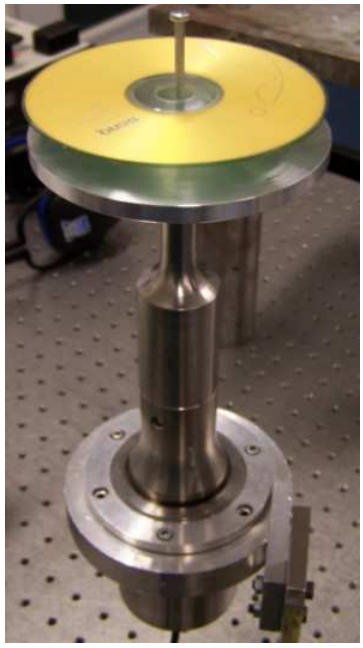

Fig. 8 Stable levitation of CD at half wavelength ($\lambda/2$) above the radiator. The central pin (screwed into the flexural plate) is used only for centering the plate in radial direction

A common compact disc (CD) is chosen as the object to be levitated. It has the same diameter as the vibrating plate, with a thickness of 1.3 mm and a mass of 16 g. A stable levitation state is observed when the input power reaches about 30 W (see Fig. 8). The CD then rests without any instable vertical motion above the flexural plate. Maximum vibration amplitude of the excitation system occurs at the center of the flexural plate and is about 25 μm at 19 kHz for this level of power (measured using a laser vibrometer). It is worth mentioning that the CD in this arrangement rests at a position slight higher than half a wavelength (above the peak of the levitation force), where the levitation force equals the gravity force of the CD. This is different compared to common radiator-reflector-type systems, in which small particles are levitated at positions slightly below the pressure nodes of the standing wave. Stable levitation could not be achieved at one wavelength or higher positions with the proposed setup due to the quickly dropped levitation force.

4.1 Sound field visualization

Visualization of sound wave propagation and interaction with structures in the levitation mechanism is important for understanding the underlying acoustics. The conventional method to measure acoustic fields with microphones is difficult in the presented system, because the measuring volume is limited, high resolution is required, and disturbances due to sensors are not acceptable. Recently, Zipser et al. [51], [50] introduced a new method for planar visualization of acoustic sound waves in gases by means of a scanning laser vibrometer. With this high sensitive method, multi-frequency, repetitive sound fields can be measured. This measurement technique is applied to study the sound field excited by the disc-shaped radiator and the interaction with the levitated objects. Since pictures of the qualitative distribution of pressure are sufficient here, no complicated post-processing is needed. A detailed descriptions of the measurement technique called refracto-vibrometry and an explanation of the underlying theory can be found in [49].

In the first experiment, the sound propagation from the vibrating radiator is visualized and shown in Fig. 9(a). Red color (darker color) indicates high pressure and green (brighter color) indicates low pressure; in an additional animated video the continuous propagation of the sound-wave has been

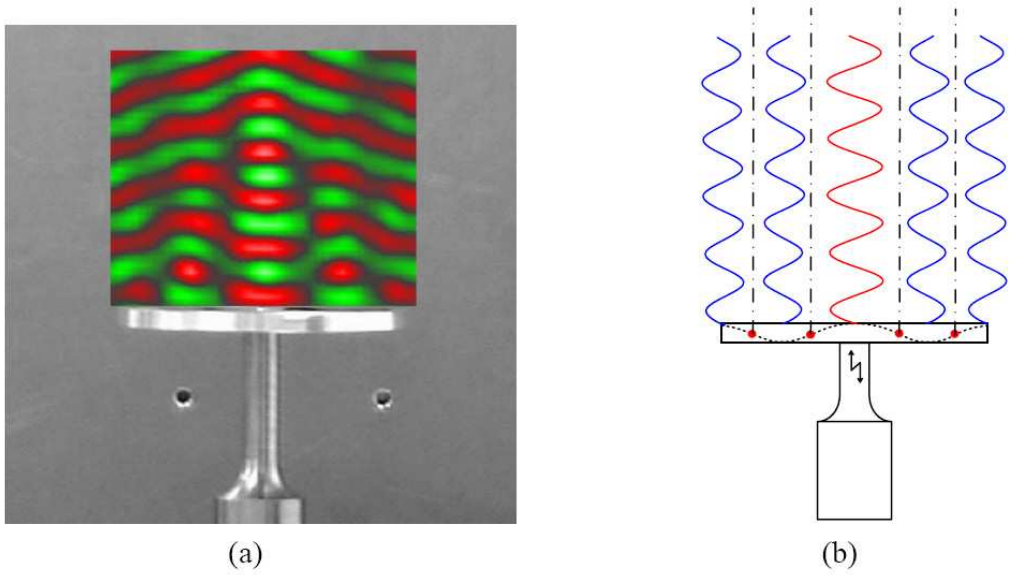

Fig. 9 Sound wave free propagation above the radiator. a) measurement result; b) schematic diagram

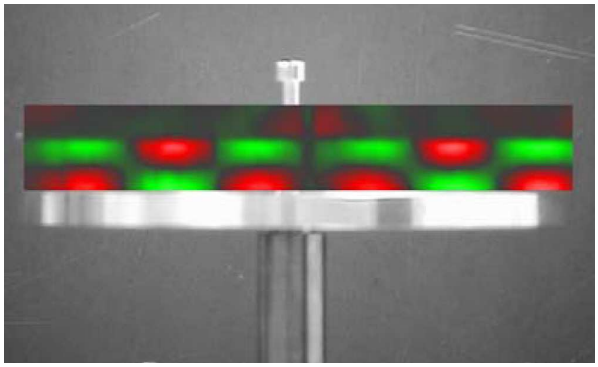

Fig. 10 Visualization of the standing wave field during stable levitation, operating frequency 19 kHz

visualized as schematically depicted in Fig. 9(b). Distinctive high and low pressure regions can be seen above the radiation surface within the first wavelength. Several interference patterns are observed starting from the second wavelength, which are typical for the acoustic near-field of this kind of radiators. The interfering regions coincide with the positions of the two nodal circles on the surface of the radiating plate as shown in Fig. 9(b).

Fig.10 shows the results measured when the CD is levitated and rests in a stable position slightly above half a wavelength. A clear standing wave pattern is seen in an animated depiction. Leak of sound pressure from the center hole of the CD is also observed. It can be stated that the levitated CD itself acts as a reflector for building the $\lambda/2$ standing wave between plate and the CD. The distinct high-low pressure distribution follows exactly the vibration mode of the radiator, which proves that the assumption made for the sound field model is acceptable.

5 Results and discussion

5.1 Computing the levitation force

To calculate the radiation pressure using Equ. 29, one needs first to know the acoustic pressure amplitude A_0. However, the acoustic pressure is difficult to measure in the presented arrangement due to the limited space. On the other hand, the mechanical vibration is much easier to obtain. The following arrangement is made to link the radiation pressure with the mechanical vibration of the radiation.

The magnitudes of air particle velocity $|\hat{\mathbf{v}}_{r,z}|$ at each point according to r and z directions can be derived from Equ. 25 as

$$|\hat{\mathbf{v}}_{r,z}| = \frac{A_0 Z(r)}{\rho_0 c} \cdot \sqrt{(\cos kz \cdot \sinh \alpha' z)^2 + (\sin kz \cdot \cosh \alpha' z)^2} = \frac{A_0 Z(r)}{\rho_0 c} \cdot \sqrt{\sinh^2 \alpha' z + \sin^2 kz} \quad (30)$$

When $z = L$ and $r = 0$ in Equ. 30, $|\hat{\mathbf{v}}_{0,L}|$ indicates the air particle speed magnitudes directly on the center of the sound radiator. Assuming that the air particles on the radiation surface move in the same way as the surface itself, $|\hat{\mathbf{v}}_{0,L}|$ is equal to surface vibration speed amplitude at the center of the radiator, represented by V_0. Therefore, the acoustic pressure amplitude A_0 at $r = 0$ can be derived from Equ. 30 as

$$A_0 = V_0 \rho_0 c / \sqrt{\sinh^2 \ \alpha' L + \sin^2 \ kL} \quad (31)$$

Equ. 31 gives a relation between the mechanical vibration of the radiator and the acoustic field. It can be seen that for a given distance L and the surface vibration amplitude V_0 at $r = 0$, the acoustic pressure amplitude A_0 at $r = 0$ can be obtained. Substituting Equ. 31 into Equ. 29, we find

$$p_{ra} = Z(r)^2 \frac{V_0^2 \rho_0}{4\left(\sinh^2 \alpha' L + \sin^2 kL\right)} \quad (32)$$

5.2 Simulation results

A normal laboratory condition with temperature of 20 degree Celsius and relative humidity of 30% is used for all the claculations in this section. α is calculated as 0.58 suing Equ. 17. In Equ. 32, all the parameters except V_0 and α' are known for a given experiment setup. V_0 can be measured experimentally during operation. α' depends on α and the wave properties. The acoustic radiation pressure can be calculated using Equ. 22 and Equ. 32. The levitation force can be obtained then by integrating p_{ra} on the surface of the levitated object.

Fig. 11 shows the radiation pressure changes with different distances between the radiator and the reflector. Y axis is radiation pressure at the center of the reflector (p_{ra}^0) caused by the center (near $r = 0$) of the sound beam. The vibration speed amplitude V_0 at the center of the radiator used for this calculation is 3 m/s. In the figure, p_{ra}^0 is normalized by the atmospheric pressure P_0 and the levitation distance is normalized by the sound wavelength. It can be seen that, the radiation pressure is normally very small compared to the atmospheric pressure. However, at intervals of half wavelength, clear peaks happen due to the formation of standing wave. When L is close to zero, the squeeze film effect takes place, and the resulted pressure increases quickly to a maximum value of 0.4 times of the atmospheric pressure.

The distribution of the radiation pressure on a circular surface with $r = 0.06$ m (as in the experiment setup presented in the preceding section) is shown in Fig. 12. The radiation pressure p_{ra} is normalized by the radiation pressure at the center of the plate p_{ra}^0. The radial distribution of the amplitude of p_{ra} follows the square of the surface vibration amplitude. At the nodal circles of the radiator, the radiation pressure drops to zero. The levitation force is obtained by integrating p_{ra} along r. Results of calculated levitation forces for different L values are plotted in Fig. 13. The measured results are plotted together with the calculated ones. It can be seen that the calculated levitation forces agree well with the measurements. However, the magnitude at the position of half wavelength is about 5

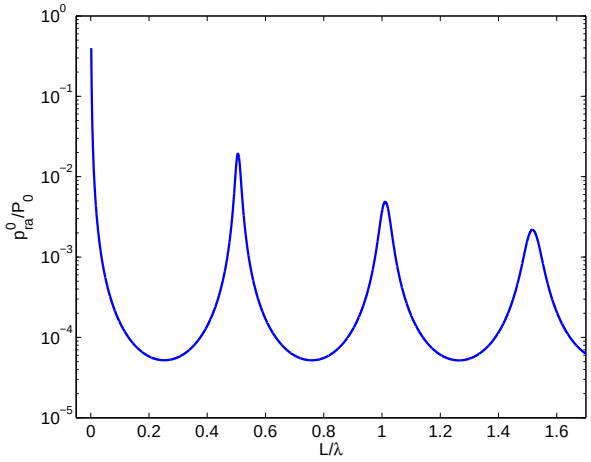

Fig. 11 Change of the radiation pressure at the center of the reflector with different distances

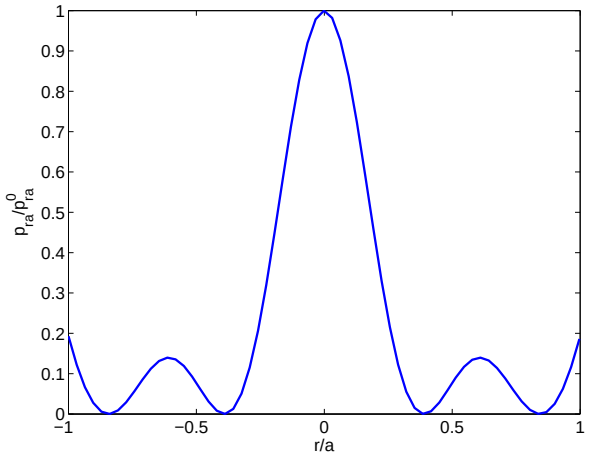

Fig. 12 Radiation pressure distribution along the surface of the reflector

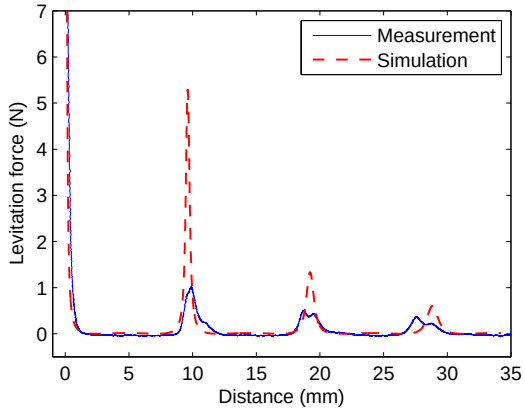

Fig. 13 Levitation force versus levitation distance, experiment and calculation results

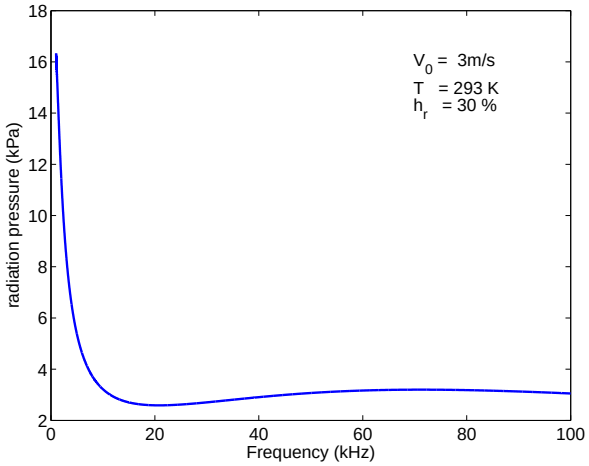

Fig. 14 Radiation pressure versus frequency, constant vibration speed

time of the measured value. The possible reasons of the higher calculated force are as following. First, the reflector used in experiment is never a perfect reflecting surface. Diffraction and absorption always exist at the reflector. Secondly, in the experiment, the two plates are not perfectly parallel. Thus, the standing wave is not formed at one single distance, but in a small range. This has been proved by the multiple peaks measured in experiment discussed in Sec. 4. Therefore, the resulted levitation force is more distributed with a smaller amplitude compared to the simulation.

For the proposed acoustic levitation system, it is interesting to know how the frequency affects the levitation force. In order to show the relation, the maximum radiation pressure (at $r = 0$) is calculated with different frequencies. For consistency, the surface vibration velocity is set constantly as $V_0 = 3$ m/s. The vibration speed is an indication of the output power of the radiator. Therefore, it can be considered that the output sound power is kept approximately constant. Fig. 14 shows the calculation results. From the figure, one can see that the radiation pressure in audible range (≤ 20 kHz) increases quickly with decreasing frequency. However, in the low frequency range (≤ 5 kHz), vibration speed of 3 m/s will require a very large displacement of the radiator. This is often not feasible in practice and will be unbearably loud. For the ultrasonic frequency range (≥ 20 kHz), the radiation pressure is rather not so sensitive to the frequency, and can be increased slightly by using higher driving frequencies. Therefore, the proposed experiment setup can be optimized by redesign the system to work at around 60 kHz.

6 Conclusion

An one dimensional acoustic levitation system for large planar objects is discussed in this paper. Basic principles behind the standing wave and squeeze film type acoustic levitation systems are reviewed. A different configuration of acoustic levitation system is presented which can levitate planar objects with dimensions much larger than the sound wavelength at a position much higher than squeeze film levitation system. Mathematical model for the pretended system is developed based on acoustic theory. Nonlinear absorption effect is taken into account in the model which makes the model fit better to the experiment. Experimental investigations are conducted to verify the levitation method. A CD is successfully levitated with the proposed system at a height of half a wavelength. The levitation forces at different distances are measured. A force of about 1 N is observed at the position of half wavelength in front of the sound radiator. Various simulation results are presented which show good agreement with the experiment result. The simulation results give good insights of the influences of different parameters on the levitation force, such as frequency and vibration models.

References

1. Abramov O (1998) High-intensity ultrasonics: theory and industrial applications. Gordon and Breach Science Publishers
2. Barmatz M, Collas P (1985) Acoustic radiation potential on a sphere in plane, cylindrical, and spherical standing wave fields. Acoustical Society of America Journal 77:928–945
3. Bass HE, Sutherland LC, Zuckerwar AJ (1990) Atmospheric absorption of sound: Update. The Journal of the Acoustical Society of America 88(4):2019–2021
4. Bass HE, Sutherland LC, Zuckerwar AJ, Blackstock DT, Hester DM (1995) Atmospheric absorption of sound: Further developments. The Journal of the Acoustical Society of America 97(1):680–683
5. Blevins RD (2001) Formulas for Natural Frequency and Mode Shape. Malabar,Florida: Krieger Publishing.
6. Bücks K, Müller H (1933) Über einige Beobachtungen an schwingenden Piezoquarzen und ihrem Schallfeld. Z Phys 84:75–86
7. Chu BT, Apfel RE (1982) Acoustic radiation pressure produced by a beam sound. Acoustical Society of America Journal 72:1673–1687
8. Chu BT, Apfel RE (1984) Response to the Comments of Nyborg and Rooney [J. Acoust. Soc. Am. 75, 263-264 (1984)] . Acoustical Society of America Journal 75:1003–1004
9. Daidzic N (1995) Nonlinear droplet oscillations and evaporation in an ultrasonic levitator. PhD thesis, Lehrstuhl fuer Stroemungsmechanik, Friedrich-Alexander-Universitaet Erlangen
10. Embleton TFW (1954) Mean Force on a Sphere in a Spherical Sound Field. I. (Theoretical). Acoustical Society of America Journal 26:40
11. Gabay R, Bucher I (2006) Resonance tracking in a squeeze-film levitation device. Mechanical Systems and Signal Processing 20:1696–1724
12. Gor'kov LP (1962) On the Forces Acting on a Small Particle in an Acoustical Field in an Ideal Fluid. Soviet Physics Doklady 6:773
13. Hasegawa T (1969) Acoustic-Radiation Force on a Solid Elastic Sphere. Acoustical Society of America Journal 46:1139
14. Hashimoto Y, Koike Y, Ueha S (1996) Near-field acoustic levitation of planar specimens using flexural vibration. Acoustical Society of America Journal 100:2057–2061
15. Höppner J (2002) Verfahren zur berhrungslosen handhabung mittels leistungsstarker schallwandler (in German). PhD thesis, Technische Universität München
16. Hu J, Nakamura K, Ueha S (1997) analysis of a noncontact ultrasonic motor with an ultrasonically levitated rotor. Ultrasonics
17. Ide T, Friend JR, Nakamura K, Ueha S (2005) A Low-Profile Design for the Noncontact Ultrasonically Levitated Stage. Japanese Journal of Applied Physics 44:4662
18. King L (1934) On the acoustic radiation pressure on spheres. Proc R Soc London Ser
19. Lee CP, Wang TG (1993) Acoustic radiation pressure . Acoustical Society of America Journal 94:1099–1109
20. Lierke E (March 1996) Acoustic levitation a comprehensive survey of principles and applications. Acta Acustica united with Acustica 82
21. Lierke L, Grossbach R, Clancy P (1983) Acoustic positioning for space processing of materials science samples in mirror furnaces. In: 1983 IEEE Ultrasonic Symposium Proceedings, p 1129
22. Littmann W (2003) Piezoelektrische, resonant betriebene Ultraschall-Leistungswandler mit nichtlinearen mechanischen Randbedingungen (in German). PhD thesis, University of Paderborn, Heinz Nixdorf Institute
23. Littmann W, Hemsel T, Kauczor C, Wallaschek J, Sinha M (2003) Load-adaptive phase-controller for resonant driven piezoelectric devices. In: World Congress Ultrasonics, Paris
24. Ma DY, Shen H (2006) Handbook of Acoustics. Science Press
25. Minikes A, Bucher I (2003) Coupled dynamics of a squeeze-film levitated mass and a vibrating piezoelectric disc: numerical analysis and experimental study. Journal of Sound Vibration 263:241–268
26. Minikes A, Bucher I, Haber S (2004) Levitation force induced by pressure radiation in gas squeeze films. Acoustical Society of America Journal 116:217–226
27. Nomura H, Kamakura T, Matsuda K (2002) Theoretical and experimental examination of near-field acoustic levitation. Acoustical Society of America Journal 111:1578–1583
28. Otsuka T, Higuchi K, Seya K (1989) Ultrasonic levitation by stepped circular vibrating plate. In: The 10th Symposium on Ultrasonic Electronics, p 170
29. Poynting JH, Thomson JJ (1904) A Textbook of Physics. Charles Griffin & Co.
30. Rayleigh L (1902) On the pressure of vibrations. Philosophical magazine 3:338
31. Reinhart R, Höppner J, Zimmermann J (2001) Non-contact wafer handling using high-intensity ultrasonics. In: IEEE/SEMI Advanced Semiconductor Manufacturing Conference, pp 139–140
32. Rossing TD (2007) Springer Handbook of Acoustics. Springer New York
33. Salbu E (1964) Compressible squeeze films and squeeze bearings. Journal of Basic Engineering 86:355–366
34. Sherman CH, Butler JL (2007) Transducers and Arrays for Underwater Sound. Springer Publishing Company, Incorporated
35. Stolarski T (2006) Self-lifting contacts: from physical fundamentals to practical applications. Proceedings of the I MECH E Part C Journal of Mechanical Engineering Science 220:1211–1218(8)
36. Trinh EH (1985) Compact acoustic levitation device for studies in fluid dynamics and material science in the laboratory and microgravity. Review of Scientific Instruments 56:2059–2065
37. Ueha S, Hashimoto Y, Koike Y (2000) Non-contact transportation using near-field acoustic levitation. Ultrasonics 38

38. Vandaele V, Lambert P, Delchambre A (2005) Non-contact handling in microassembly: Acoustical levitation. Precision Engineering 29:491–505
39. Wang T, Saffren M (1974) Acoustic chamber for weightless positioning. AIAA paper 155
40. Westervelt PJ (1950) The mean pressure and velocity in a plane acoustic wave in a gas. Acoustical Society of America Journal 22:319–327
41. Westervelt PJ (1951) The Theory of Steady Forces Caused by Sound Waves. Acoustical Society of America Journal 23:312–315
42. Westervelt PJ (1957) Acoustic radiation pressure. Acoustical Society of America Journal 29:26–29
43. Whymark R (1975) Acoustic field positioning for containerless processing. Ultrasonics 13:251–261
44. Wiesendanger M (2001) Squeeze film air bearings using piezoelectric bending elements. PhD thesis, Ecole polytechnique federale de Lausanne
45. Xie WJ, Wei B (2001) Parametric study of single-axis acoustic levitation. Applied Physics Letters 79:881
46. Xie WJ, Wei B (2004) Dynamics of acoustically levitated disk samples. Physical Review 70(4):046,611
47. Xie WJ, Cao CD, Lü YJ, Hong ZY, Wei B (2006) Acoustic method for levitation of small living animals. Applied Physics Letters 89(21):214,102
48. Yoshimoto S, Kobayashi H, Miyatake M (2007) Float characteristics of a squeeze-film air bearing for a linear motion guide using ultrasonic vibration. Tribology Inter 40:503–511
49. Zipser L (2006) Refraktovibrometrie zur Messung und Visualisierung akustischer, fluidischer und spannungsmechanischer Phenomene. In: 9. Polytec Vibrometer Seminar, Waldbronn
50. Zipser L, Lindner S (2001) Visualisation of vortexes and acoustic sound waves. In: Proceedings of 17th Int. Congress on Acoustics, vol I, Physical Acoustics part B, Ultrasonics, quantum acoustics and physical effect of sound, pp 24–25
51. Zipser L, Lindner S, Behrendt R (23) Anordnung zur Messung und visuellen Darstellung von Schalldruckfeldern (Equipment for measurement and visualisation of sound fields). Patent DE 10 057 922